The impact of magnetite nanoparticles on the physicochemical and adsorption properties of magnetic alginate beads

Georges Germanos, Sami Youssef, Wehbeh Farah, Benoit Lescop, Stéphane Rioual, Maher Abboud

▶ **To cite this version:**

Georges Germanos, Sami Youssef, Wehbeh Farah, Benoit Lescop, Stéphane Rioual, et al.. The impact of magnetite nanoparticles on the physicochemical and adsorption properties of magnetic alginate beads. Journal of Environmental Chemical Engineering, 2020, 8 (5), pp.104223. 10.1016/j.jece.2020.104223 . hal-02943738

HAL Id: hal-02943738
https://hal.science/hal-02943738v1

Submitted on 2 Oct 2024

HAL is a multi-disciplinary open access archive for the deposit and dissemination of scientific research documents, whether they are published or not. The documents may come from teaching and research institutions in France or abroad, or from public or private research centers.

L'archive ouverte pluridisciplinaire **HAL**, est destinée au dépôt et à la diffusion de documents scientifiques de niveau recherche, publiés ou non, émanant des établissements d'enseignement et de recherche français ou étrangers, des laboratoires publics ou privés.

The impact of magnetite nanoparticles on the physicochemical and adsorption properties of magnetic alginate beads

G. Germanos[a,*], S. Youssef[b], W. Farah[a], B. Lescop[c], S. Rioual[c], M. Abboud[a]

[a] Université Saint-Joseph, Unité Environnement Génomique et Protéomique - UEGP, Faculté des Sciences, Campus des Sciences et Technologies, Mar Roukoz – B.P. 1514 Riad El Solh Beyrouth, 1107 2050, Lebanon
[b] Université Saint-Joseph, Ecole supérieure d'ingénieurs de Beyrouth, Campus des Sciences et Technologies, Mar Roukoz, B.P. 1514 - Riad El Solh Beyrouth, 1107 2050, Lebanon
[c] Univ Brest, Lab-STICC, CNRS, UMR 6285, F-29200, Brest, France

ARTICLE INFO

Keywords:
Magnetic alginate beads
Nanoparticles
Physicochemical characterization
Copper adsorption

ABSTRACT

In this study, calcium alginate-based adsorbents with magnetic and non-magnetic properties (MABs and ABs) were prepared and the impact of the incorporated magnetite nanoparticles (Fe_3O_4 NPs) on the physicochemical properties, adsorption kinetics and Cu(II) uptake mechanism was determined. ABs and MABs were characterized by X-ray diffraction (XRD), scanning electron microscopy (SEM), thermogravimetric analysis (TGA) and superconducting quantum interference device magnetometer (SQUID). The SEM analysis of the MABs showed that the composite has a rough surface with abundant protuberances. The XRD analysis showed an amorphous structure of the ABs. The TGA analysis revealed higher thermal stability of the MABs compared to ABs. The MABs proved to be superparamagnetic at room temperature. The adsorption experiments of copper ions onto ABs and MABs were also carried out. It was revealed that for the same weight of the alginate matrix, the MABs and the ABs have an adsorption efficiency of 54.9 and 66.7 mg/g, respectively. The adsorption kinetics were followed by a pseudo-second-order kinetic model and the diffusion properties played a significant role in the control of the adsorption kinetics. The adsorption equilibrium rate constant (k_2) for the pseudo-second-order model was found to be 1.98×10^{-4} g. mg^{-1}. min^{-1} for ABs and 3.8×10^{-4} g. mg^{-1}. min^{-1} for MABs.

1. Introduction

Many industrial activities involve the discharge of metallic ions such as copper, silver or zinc which contributes to waste contamination [1]. Considering the related environmental damages and impact on human health, there is a rising global interest in the removal of such ions from wastewater [2]. Various methods are used for this purpose such as ion exchange [3], chemical precipitation [4], electrochemical [5,6], flotation [7], membrane filtration [8] and adsorption [9]. Among these techniques, the adsorption of metallic ions by active materials is considered as a simple and effective method. For decades, activated carbons were used for water remediation. These materials present several advantages, notably a large specific surface area, a high adsorption capacity, remarkably high reactivity, and a porous structure [10]. However, the main drawbacks of these materials are high cost and constraints of regeneration [11]. Alternatively, the adsorption of ions by biopolymer is considered as a promising technique given due to its low cost, high efficiency and eco-friendly [12]. In particular, alginate biopolymer is inexpensive and displays excellent cation adsorption properties due to the presence of numerous functional groups such as COOH and OH groups. Therefore, alginate beads (ABs) were used for the remediation of several heavy metals [13–19]. Magnetic nanoparticles can also be integrated into the polymer, authorizing thereby the use of magnetic separation method to separate the composite biosorbent from the wastewater. Recently, many studies have reported the incorporation of magnetite (Fe_3O_4) or maghemite (Fe_2O_3) nanoparticles in the polymer for ions sorption [20–26]. Similar, magnetic alginate beads (MABs) crosslinked with epichlorohydrin were also used for dye removal [27]. Most of these studies focused on the ability of the pseudo-second-order to describe the kinetics of adsorption by MABs and only few studies report the influence of magnetic nanoparticles on the adsorption process [24,29]. In contrast, our previous work [29] demonstrates clearly that copper adsorption initiates the migration and agglomeration of iron nanoparticles in MABs.

The present study aims therefore at comparing the kinetics of adsorption of copper by MABs and ABs to highlight the influence of iron

* Corresponding author.
E-mail address: georges.germanos@usj.edu.lb (G. Germanos).

nanoparticles on the kinetic of adsorption. For this purpose, we have used sodium alginate (SA) and magnetic nanoparticles to produce ABs and MABs which present a high adsorption capacity for Cu(II). The physicochemical properties of materials are characterized by scanning electron microscopy (SEM), X-ray diffraction (XRD), thermogravimetric analysis (TGA) and superconducting quantum interference device magnetometer (SQUID). The kinetics of adsorption of MABs and ABs elaborated with the same weight of alginate are compared with second-order and intraparticle diffusion [28] models. A faster adsorption kinetic of copper ions by MABs is highlighted with respect to ABs and discussed.

2. Materials and methods

2.1. Chemicals

Sodium alginate (SA), copper (II) sulfate pentahydrate ($CuSO_4$, $5H_2O$), hydrochloric acid (37 % aqueous solution), sodium hydroxide (NaOH), iron oxide nanoparticles with particle size below 50 nm purchased from Sigma Aldrich. Calcium chloride dihydrate ($CaCl_2$, $2H_2O$) supplied by Fluka was used as a crosslinking agent for the alginate. All chemicals were bought in analytical purity and used without further purification.

2.2. Preparation of ABs and MABs

ABs and MABs were prepared according to the previously reported methods [29]. The SA solution was prepared by adding 0.75 g of SA into 50 mL of distilled water under vigorous stirring for 30 min at 80 °C. The ABs with appropriate physical stability were prepared following a simple protocol whereby the viscous alginate solution was added dropwise into 100 mL of 2% $CaCl_2$ bath under gentle stirring at room temperature. This led to the precipitation of the alginate droplets due to the ionic crosslinking properties of Ca^{2+} ions. The preparation of the MABs followed a similar process except for the incorporation of 20 % (w/w) magnetite into the SA solution and was subsequently placed in an ultrasonic bath for 90 min at room temperature forming a homogeneous mixture and extruding dropwise into the calcium chloride bath. The obtained beads are spherical (Fig. 1) with an average diameter of 2 mm as confirmed by optical microscopy under ×10 magnification. The produced ABs and MABs were then allowed to rest and harden for 24 h at room temperature without agitation. These were then filtered and rinsed with deionized water several times to remove the excess of calcium and were finally dried in an oven at 55 °C for 2 days.

Fig. 1. Magnetic alginate beads.

As mentioned above, the experiments conducted in this research paper are based on MABs incorporating 20 % of magnetite (w/w). However, and for comparative purposes pertaining to beads morphology, a single experiment introducing 5% of magnetite (w/w) was exclusively conducted in SEM analysis.

2.3. Characterization

The X-ray diffraction *(XRD – PANalytical EMPYREAN)* patterns were recorded with a diffractometer equipped with Cu K α radiation source (λ= 0.15406 nm) at a step size of 0.05°. The morphology of the alginate beads was observed by scanning electron microscopy *(SEM – Hitachi S800)*. The samples were then characterized using Thermogravimetric analysis *(Thermal Analysis – TGAQ50)* under normal atmosphere. The magnetic properties of the beads were investigated using a superconducting quantum interference device magnetometer *(SQUID – MPMS – XL – 7 T)* at room temperature. The copper concentration was quantified by atomic absorption spectrophotometer *(AAS – Thermo Elemental ASX-510)*.

2.4. Adsorption kinetics experiments

The adsorption experiments were performed for 30 h of contact time at a stable temperature of 25 °C by shaking the adsorption mixture at 250 rpm with 0.24 g of ABs and 0.30 g of MABs. This weight of MABs was selected since it corresponds to the same weight of alginate (0.24 g) plus the additional weight (0.06 g) of magnetic nanoparticles. The initial concentration of Cu(II) in the solution was set at 75 mg/L. The pH of the solution was measured at the beginning and the end of each experiment and was maintained at an optimal pH of 5.1 using sodium hydroxide or hydrochloric acid. The sampling process involved two stages. In stage one, samples were taken at regular time intervals of 10 min within the first two hours. In stage two, the sampling process occurred mainly every 3 h until reaching the time limit of 30 h. During the AAS measurements, the adsorption capacity (q_t) is defined as the amount of copper cations adsorbed per unit mass of adsorbent at any time. It is given by the relation:

$$q_t = \frac{(C_0 - C_t)\,V}{W} \quad (1)$$

where C_0 is the initial copper solution concentration, C_t the concentration at the time t, V the volume of the copper solution, and W the total weight of the adsorbent.

3. Results and discussion

3.1. Morphology of the beads

Figs. 2(a–d) displays the morphology of the alginate beads by using scanning electron microscopy. Figs. 2(a) and 2(b) show the SEM images of ABs at 150 and 1000x magnification, respectively. A smooth, homogenous and groovy surface is then observed. This result contrasts with the images obtained on MABs on Figs. 2(c,d) which show an irregular and rough surface. As seen, by comparing Fig. 2(c) and 2 (d), increasing the amount of magnetite nanoparticles from 5% to 20 % in the beads increase strongly the number of protuberances which appear at the surface.

3.2. Crystallographic characteristics of the beads

Fig. 3 shows the XRD patterns of Fe_3O_4 NPs, MABs and ABs. A series of characteristic peaks for Fe_3O_4 NPs were observed at 2θ of 30.1, 35.6, 43.2, 53.7, 57.4 and 62.7°, corresponding to (220), (311), (400), (422),

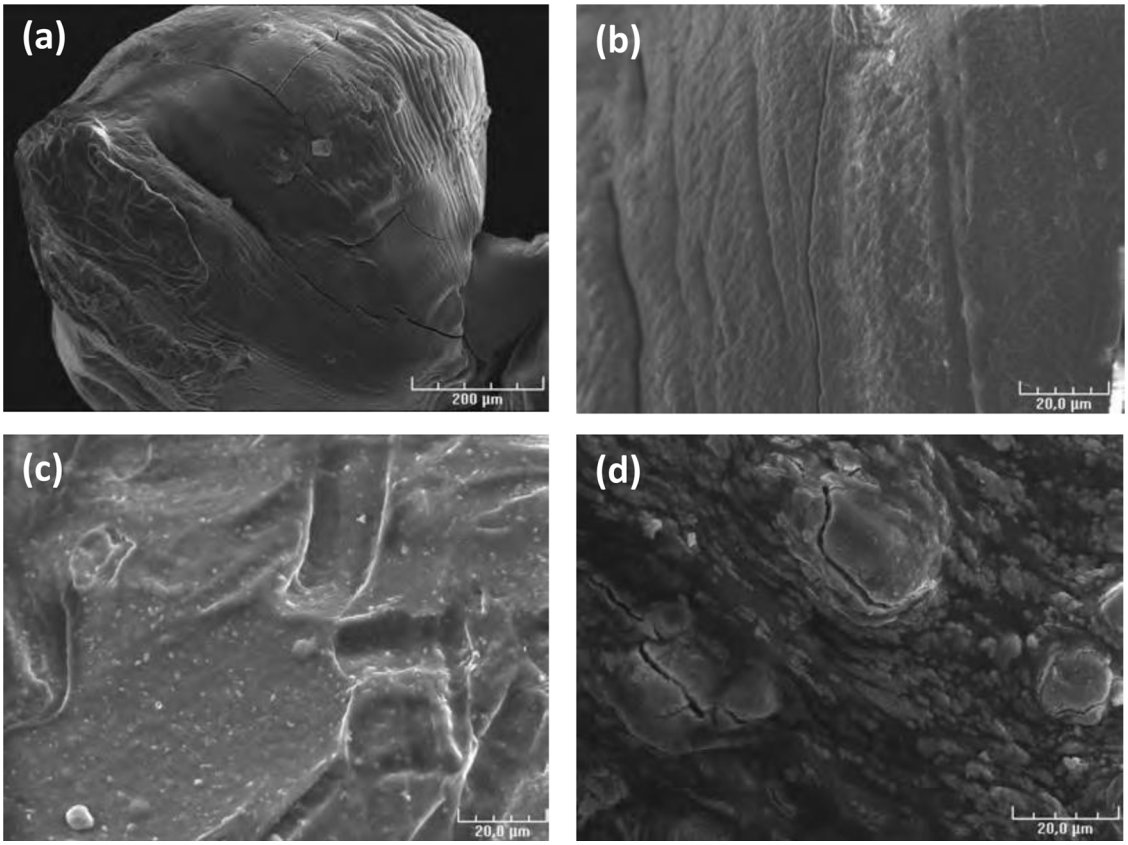

Fig. 2. Scanning electron micrographs of : (a) and (b) alginate beads; (c) magnetite alginate beads with 5% of magnetite; (d) magnetite alginate beads with 20 % of magnetite.

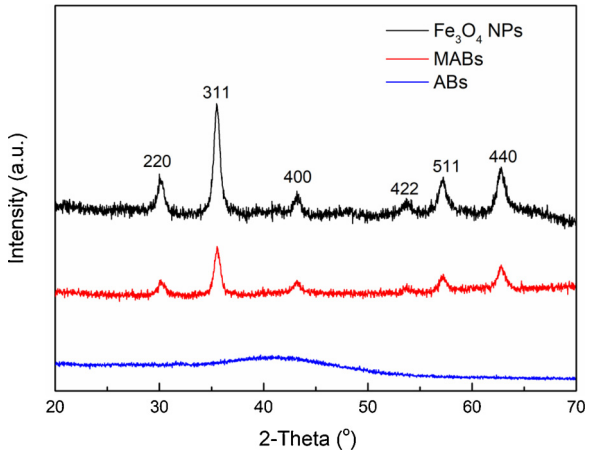

Fig. 3. X-ray diffraction (XRD) patterns of magnetic alginate beads, pure alginate beads and magnetite NPs.

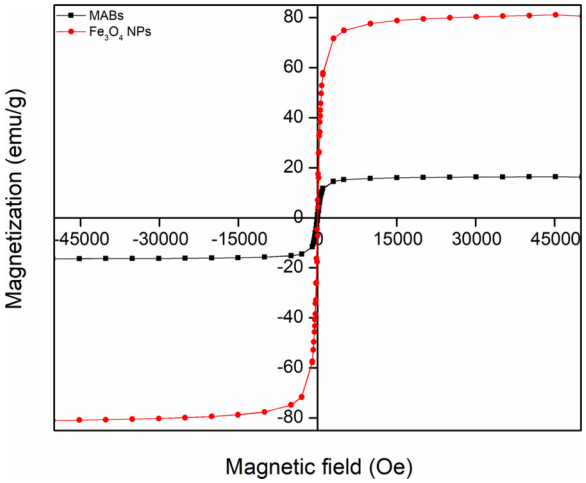

Fig. 4. Magnetization vs. applied magnetic field of magnetite NPs and magnetic alginate beads.

(511) and (440) crystalline planes of magnetite phase, respectively [30]. The peak intensity of MABs is lower than that of the pure Fe_3O_4 NPs. This is explained by the fact that Fe_3O_4 NPs are incorporated into the polymer matrix. The XRD pattern of ABs shows a single broad diffused peak which suggests the presence of an amorphous phase [31].

3.3. Magnetic properties of Fe_3O_4 NPs and MABs

The magnetization curves measured at room temperature for Fe_3O_4 NPs and MABs are depicted in Fig. 4. There was no hysteresis and coercivity in the magnetization for both of Fe_3O_4 NPs and MABs samples suggesting that magnetic nanoparticles and MABs are superparamagnetic and the single domain magnetite nanoparticles remained in the polymer composite. This can be attributed to the relatively smaller size of the magnetite nanoparticles which compared to the superparamagnetic critical size [32]. The saturation magnetization value (M_s) of MABs was 80 % lower than the value of the pure magnetite nanoparticles and decreased from 81 to 16.3 emu/g [33]. This was due to the low content of Fe_3O_4 nanoparticles in the MABs with 20 % (w/w) of magnetite. This suggests that the magnetization of the MABs is independent of the alginate matrix. With the displayed magnetization and superparamagnetic behaviors, the MABs could be easily and rapidly separated from the solution by an external magnetic field.

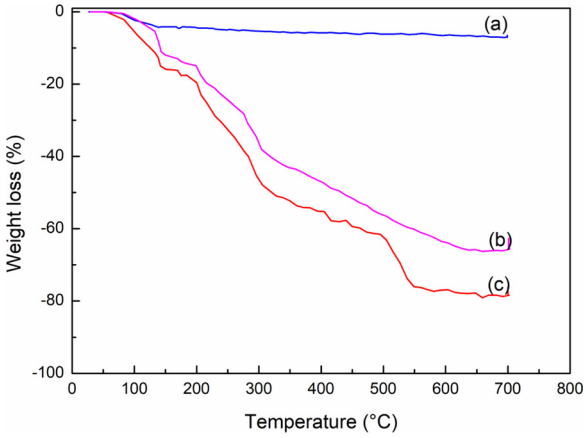

Fig. 5. TGA curves of (a) Fe_3O_4 NPs, (b) MABs and (c) ABs.

Therefore, these magnetic properties are of critical importance in the wastewater treatment by magnetic separation.

3.4. TGA analysis

Fe_3O_4 NPs, MABs and ABs were characterized using TGA under normal atmosphere from room temperature up to 700 °C, the heating rate was set at 4 °C/min. The results are illustrated in Fig. 5 and show three main processes of weight loss for both adsorbent. The first process ranging from 50 to 150 °C is related to the evaporation of the adsorbed water molecules and the destruction of glycosidic bonds of the polysaccharide network of the alginate. This weight loss occurred more rapidly when the polymer network is used solely without the incorporation of mineral nanoparticles of magnetite that can contribute to a more thermally stable composite. The second decomposition process ranging from 150 to 300 °C showed increased weight loss and is associated with depolymerization [34]. This degradation of the polymer chains occurs at an accelerated rate when using ABs compared to MABs and is likely due to the intermolecular interaction between the chains and the magnetite nanoparticles leading to a more cohesive system. When the temperature is between 300 and 700 °C, the losses continue in the case of MABs and ABs due to the gradual and accelerated departure of the organic fragments of the alginate matrix.

3.5. Adsorption kinetics of ABs and MABs

In order to identify the kinetic mechanism of the adsorption process, three typical kinetic models were used to simulate the adsorption kinetics of Cu(II) onto ABs and MABs. The linearized form of the pseudo-first-order model, pseudo-second-order model and intraparticle diffusion model are presented as follows [35,36]:

$$\text{Pseudo-first-order equation: } \ln(q_e - q_t) = \ln(q_e) - k_1 t \quad (2)$$

$$\text{Pseudo-second-order equation: } \frac{t}{q_t} = \frac{1}{k_2 q_e^2} + \frac{t}{q_e} \quad (3)$$

$$\text{Intraparticle diffusion equation: } q_t = k_{int} t^{0.5} + X_i \quad (4)$$

where k_1 is the first-order rate constant (min^{-1}), k_2 is the second-order-rate constant ($g.mg^{-1}.min^{-1}$), q_e ($mg.g^{-1}$) the amount of copper ions adsorbed at equilibrium, q_t ($mg.g^{-1}$) the amount of copper ions adsorbed at any time t (min), k_{int} is the intraparticle diffusion rate constant ($mg.g^{-1}.min^{-0.5}$) and X_i is the boundary layer thickness (mg/g).

The obtained kinetic parameters of the pseudo-first-order, pseudo-second-order and intraparticle diffusion models were presented in Tables 1 and 2. The linear fitting results of the pseudo-first-order and the pseudo-second-order kinetic models for ABs and MABs were illustrated in Figs. 6 and 7, respectively. When comparing the correlation coefficients of the three kinetic models, it is clearly revealed that the pseudo-second-order model best fits the adsorption kinetic of Cu (II) onto ABs and MABs. In effect, the equilibrium adsorption capacity values calculated from the pseudo-second-order model are in line with the experimental data. The adsorption rate of the copper ions is therefore controlled by chemical adsorption. This higher applicability of the pseudo-second-order model over the other kinetic models is also in line with other studies where similar conclusions were reached pertaining to the kinetics of Cu(II) adsorption onto alginate-based adsorbent [37–39]. The adsorption capacity (q_t) of the adsorbent was found to be 54.9 and 66.7 mg/g for the MABs and the ABs, respectively. Taking into consideration the fact that MABs are composed of 80 % of calcium alginate and 20 % of magnetite nanoparticles, it is then possible to normalize the MABs adsorption capacity to the alginate weight. This would lead to an adsorption capacity of 68.6 mg/g for the MABs. Moreover, the adsorption equilibrium rate constant (k_2) was found to be 3.8×10^{-4} $g.mg^{-1}.min^{-1}$ for MABs and 1.98×10^{-4} $g.mg^{-1}.min^{-1}$ for ABs. The MABs show a considerable removal efficiency and faster kinetics attributed to the greater specific surface area. However, the magnetite NPs showed no interaction with the copper ions as identified by the conducted XPS analysis in our previous study [29].

Then, the intraparticle diffusion model analysis can provide further details on the rate-controlling process and can describe the adsorption process more clearly. The linear fitting results of the intraparticle diffusion model for ABs and MABs are shown in Fig. 8. According to the published literature, the plot q_t versus $t^{1/2}$ should be linear when intraparticle diffusion is involved in the adsorption process [40]. Whenever the plot crosses the origin, this would indicate that the intra-particle diffusion is the sole rate-controlling step. Otherwise, the rate-controlling process includes other mechanisms which can be operating simultaneously with the intraparticle diffusion model [41]. In this work, the analysis of the experimental data using intraparticle diffusion model (Fig. 8) revealed the presence of three linear sections of different slopes for ABs and MABs. These results indicated that the adsorption process involved three steps and the intraparticle diffusion was not the only rate-controlling process in the adsorption process of the copper ions onto ABs and MABs. The first step corresponded to an instantaneous adsorption or external surface adsorption while in the second step, a gradual uptake was observed reflecting the intraparticle diffusion as the rate-limiting step until the exterior surface reached saturation. In the third step, the final equilibrium was reached and the intraparticle diffusion slowed down due to the extremely low concentration of Cu(II) in the solution [42,43]. This finding that the intraparticle diffusion occurs at different rates in three steps has also been reported on heavy metals adsorption in previous studies [44,45].

Table 1
Pseudo-first-order and pseudo-second-order kinetic models parameters.

Types of beads	qe_{exp} (mg/g)	Pseudo-first-order			Pseudo-second-order		
		K_1 (min^{-1})	qe_{th} (mg/g)	R^2	K_2 ($g.mg^{-1}.min^{-1}$)	qe_{th} (mg/g)	R^2
ABs	66.7	1.91×10^{-3}	36.7	0.843	1.98×10^{-4}	70.1	0.997
MABs	54.9	1.2×10^{-3}	21.8	0.813	3.8×10^{-4}	55.8	0.999

Table 2
Kinetic parameters of the intraparticle diffusion model.

Types of beads	First linear stage			Second linear stage			Third linear stage		
	K_{int} (mg/g. $min^{1/2}$)	X_i (mg/g)	R^2	K_{int} (mg/g. $min^{1/2}$)	X_i (mg/g)	R^2	K_{int} (mg/g. $min^{1/2}$)	X_i (mg/g)	R^2
ABs	4.77	−7.12	0.993	1.57	30.68	0.983	0.294	55.3	0.962
MABs	3.54	1.66	0.995	1.15	27.4	0.994	0.148	47.6	0.846

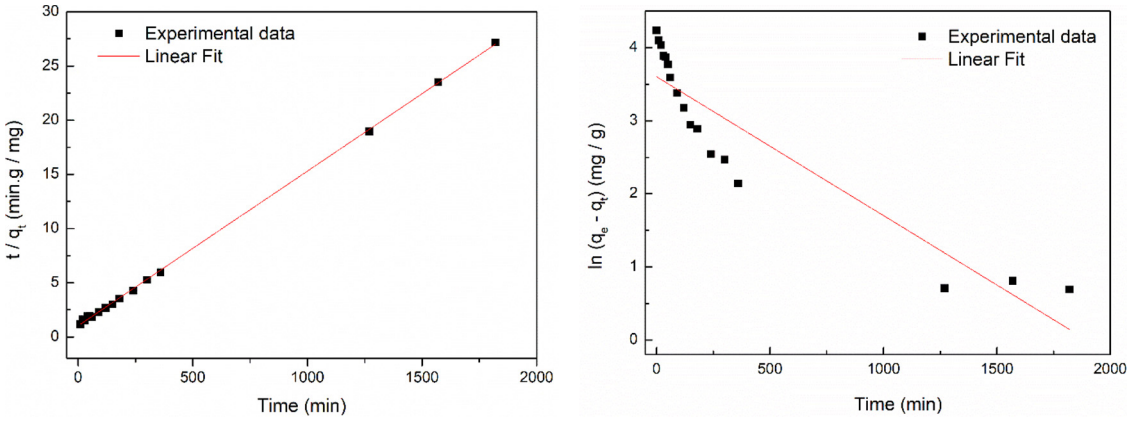

Fig. 6. Kinetics study of Cu(II) adsorption using alginate beads: (a) Pseudo-second-order model and (b) Pseudo-first order model.

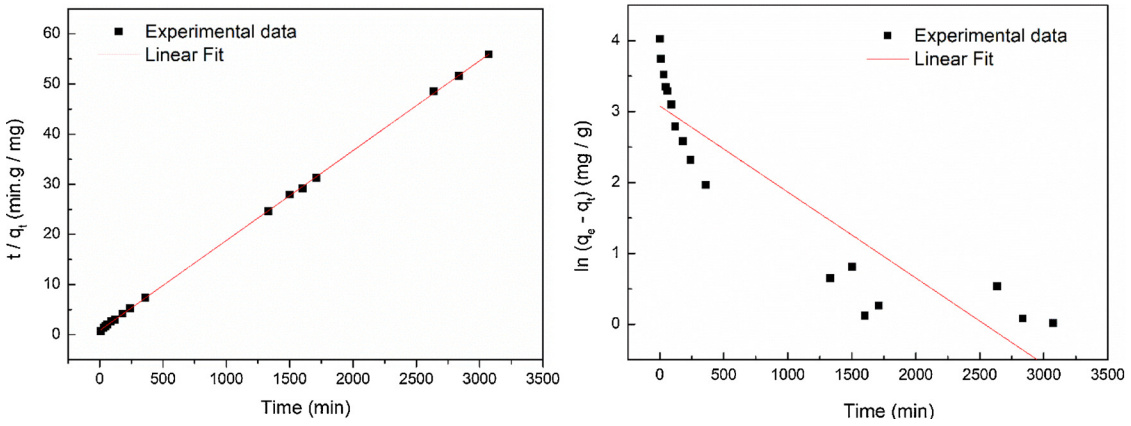

Fig. 7. Kinetics study of Cu (II) adsorption using the magnetic alginate beads: (a) Pseudo-second-order model and (b) Pseudo-first order model.

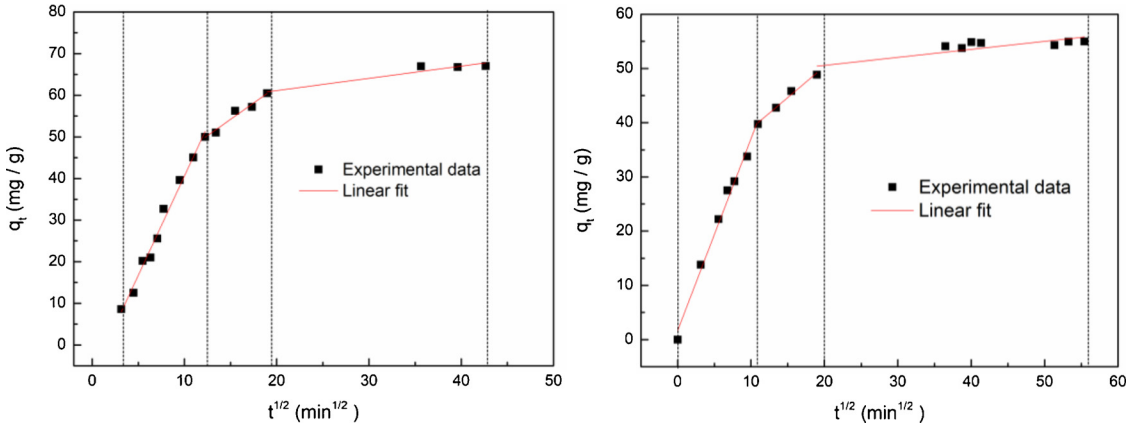

Fig. 8. Adsorption kinetics of intraparticle diffusion model for the adsorption of Cu(II) on: (a) ABs and (b) MABs.

4. Conclusion

This study showed that incorporating inorganic magnetite onto alginate matrix affects the physicochemical properties and uptake kinetics of Cu(II) onto the composite. SEM analysis showed that the MABs surface is rough while ABs surface is smooth. The magnetic properties of the magnetic beads exhibited superparamagnetism with saturation magnetization in the range of 16.3 emu/g depending on the weight load of the magnetite nanoparticles in the matrix of calcium alginate beads. TGA analysis confirmed that the incorporation of 20 wt % magnetite nanoparticles into the alginate matrix enhanced thermal stability as compared to that of ABs. The kinetic studies indicated that the pseudo-second-order model was appropriate to describe the Cu(II) adsorption process and the intraparticle diffusion was not the sole rate-controlling process. Hence, it can be suggested that the surface adsorption and intraparticle diffusion were concurrently operating. Furthermore, the results showed that the adsorption of Cu(II) ions on MABs was faster than on ABs.

CRediT authorship contribution statement

G. Germanos: Conceptualization, Formal analysis, Writing - review & editing. **S. Youssef:** Conceptualization, Funding acquisition, Supervision, Writing - review & editing. **W. Farah:** Funding acquisition, Project administration, Resources. **B. Lescop:** Methodology, Validation, Visualization, Writing - review & editing. **S. Rioual:** Methodology, Project administration, Validation, Writing - review & editing. **M. Abboud:** Conceptualization, Formal analysis, Supervision, Validation.

Declaration of Competing Interest

The authors declare that they have no known competing financial interests or personal relationships that could have appeared to influence the work reported in this paper.

Acknowledgment

This work was financially supported by the research council of Saint Joseph University (Grant number FS70 and ESIB55). The Authors gratefully acknowledge Professor Roland Habchi and Professor Michel Kazan for their valuable help.

Appendix A. Supplementary data

Supplementary material related to this article can be found, in the online version, at doi:https://doi.org/10.1016/j.jece.2020.104223.

References

[1] M.I. Zaman, S. Mustafa, S. Khan, B. Xing, Heavy metal desorption kinetic as affected by of anions complexation onto manganese dioxide surfaces, Chemosphere 77 (2009) 747–755, https://doi.org/10.1016/j.chemosphere.2009.08.030.

[2] S. Rezania, M. Ponraj, A. Talaiekhozani, S.E. Mohamad, M.F. Md Din, S. Mat Taib, F. Sabbagh, F. Md Sairan, Perspectives of phytoremediation using water hyacinth for removal of heavy metals, organic and inorganic pollutants in wastewater, J. Environ. Manage. 163 (2015) 125–133, https://doi.org/10.1016/j.jenvman.2015.08.018.

[3] S.Y. Kang, J.U. Lee, S.H. Moon, K.W. Kim, Competitive adsorption characteristics of Co^{2+}, Ni^{2+}, and Cr^{3+} by IRN-77 cation exchange resin in synthesized wastewater, Chemosphere 56 (2004) 141–147, https://doi.org/10.1016/j.chemosphere.2004.02.004.

[4] J.L. Huisman, G. Schouten, C. Schultz, Biologically produced sulphide for purification of process streams, effluent treatment and recovery of metals in the metal and mining industry, Hydrometallurgy. 8 (2006) 106–113, https://doi.org/10.1016/j.hydromet.2006.03.017.

[5] M.R. Jakobsen, L. Fritt-Rasmussen, S. Nielsen, L.M. Ottosen, Electrodialytic removal of cadmium from wastewater sludge, J. Hazard. Mater. 106 (2004) 127–132, https://doi.org/10.1016/j.jhazmat.2003.10.005.

[6] T.A. Kurniawan, G.Y.S. Chan, W.H. Lo, S. Babel, Physico-chemical treatment techniques for wastewater laden with heavy metals, Chem. Eng. J. 118 (2006) 83–98, https://doi.org/10.1016/j.cej.2006.01.015.

[7] M. Bodzek, M. Dudziak, M. Luks-Betlej, Application of membrane techniques to water purification: removal of phthalates, Desalination 162 (2004) 121–128, https://doi.org/10.1016/S0011-9164(04)00035-9.

[8] E.I. El-Shafey, M. Cox, A.A. Pichugin, Q. Appleton, Application of a carbon sorbent for the removal of cadmium and other heavy metals ions from aqueous solution, J. Chem. Technol. Biotechnol. 77 (4) (2002) 429–436, https://doi.org/10.1002/jctb.577.

[9] G.V.S.R.P. Kumar, K. Avinash, M. Bharath, Y.K. Srinivasa, Removal of Cu (II) using three low - cost adsorbents and prediction of adsorption using artificial neural networks, Appl. Water Sci. 9 (3) (2019) 1–9, https://doi.org/10.1007/s13201-019-0924-x.

[10] J. Rivera-Utrilla, M. Sánchez-Polo, V. Gómez-Serrano, P.M. Álvarez, M.C.M. Alvim-Ferraz, J.M. Dias, Activated carbon modifications to enhance its water treatment applications, An overview, J. Hazard. Mater. 187 (2011) 1–23, https://doi.org/10.1016/j.jhazmat.2011.01.033.

[11] A. Bhatnagar, W. Hogland, M. Marques, M. Sillanpää, An overview of the modification methods of activated carbon for its water treatment applications, Chem. Eng. J. 219 (2013) 499–511, https://doi.org/10.1016/j.cej.2012.12.038.

[12] M. Dechatre, B. Lescop, C. Simon Colin, F. Ghillebaert, J. Guezennec, S. Rioual, Characterization of exopolysaccharides after sorption of silver ions in aqueous solution, J. Environ. Chem. Eng. 3 (2015) 210–216, https://doi.org/10.1016/j.jece.2014.09.021.

[13] D. Chen, Z. Lewandowski, F.P. Roe, P. Surapaneni, Diffusivity of Cu^{2+} in calcium alginate gel beads, Biotechnol. Bioeng. 41 (1993) 755–760, https://doi.org/10.1002/bit.260410710.

[14] M.M. Araújo, J.A. Teixeira, Trivalent chromium sorption on alginate beads, Int. Biodeterior. Biodegradation 40 (1997) 63–74, https://doi.org/10.1016/S0964-8305(97)00064-4.

[15] J.P. Ibáñez, Y. Umetsu, Potential of protonated alginate beads for heavy metals uptake, Hydrometallurgy. 64 (2002) 89–99, https://doi.org/10.1016/S0304-386X(02)00012-9.

[16] S.K. Papageorgiou, E.P. Kouvelos, F.K. Katsaros, Calcium alginate beads from Laminaria digitata for the removal of Cu^{+2} and Cd^{+2} from dilute aqueous metal solutions, Desalination. 224 (2008) 293–306, https://doi.org/10.1016/j.desal.2007.06.011.

[17] E. Fourest, B. Volesky, Alginate properties and heavy metal biosorption by marine algae, Appl. Biochem. Biotechnol. 67 (1997) 215–226, https://doi.org/10.1007/BF02788799.

[18] J.P. Ibáñez, Y. Umetsu, Uptake of trivalent chromium from aqueous solutions using protonated dry alginate beads, Hydrometallurgy. 72 (2004) 327–334, https://doi.org/10.1016/j.hydromet.2003.10.009.

[19] H.G. Park, M.Y. Chae, Novel type of alginate gel-based adsorbents for heavy metal removal, J. Chem. Technol. Biotechnol. 79 (2004) 1080–1083, https://doi.org/10.1002/jctb.1080.

[20] S.F. Lim, Y.M. Zheng, S.W. Zou, J. Paul Chen, Removal of copper by calcium alginate encapsulated magnetic sorbent, Chem. Eng. J. 152 (2009) 509–513, https://doi.org/10.1016/j.cej.2009.05.029.

[21] A. Idris, N.S. Mohd Ismail, N. Hassan, E. Misran, A.F. Ngomsik, Synthesis of magnetic alginate beads based on maghemite nanoparticles for Pb(II) removal in aqueous solution, J. Ind. Eng. Chem. 18 (2012) 1582–1589, https://doi.org/10.1016/j.jiec.2012.02.018.

[22] X. Li, Y. Qi, Y. Li, Y. Zhang, X. He, Y. Wang, Novel magnetic beads based on sodium alginate gel crosslinked by zirconium(IV) and their effective removal for Pb^{2+} in aqueous solutions by using a batch and continuous systems, Bioresour. Technol. 142 (2013) 611–619, https://doi.org/10.1016/j.biortech.2013.05.081.

[23] S.F. Lim, J. Paul Chen, Synthesis of an innovative calcium-alginate magnetic sorbent for removal of multiple contaminants, Appl. Surf. Sci. 253 (2006) 5772–5775, https://doi.org/10.1016/j.apsusc.2006.12.049.

[24] A.F. Ngomsik, A. Bee, J.M. Siaugue, D. Talbot, V. Cabuil, G. Cote, Co (II) removal by magnetic alginate beads containing Cyanex 272, J. Hazard. Mater. 166 (2009) 1043–1049, https://doi.org/10.1016/j.jhazmat.2008.11.109.

[25] D. Wu, J. Zhao, L. Zhang, Q. Wu, Y. Yang, Lanthanum adsorption using iron oxide loaded calcium alginate beads, Hydrometallurgy. 101 (2010) 76–83, https://doi.org/10.1016/j.hydromet.2009.12.002.

[26] A. Bee, D. Talbot, S. Abramson, V. Dupuis, Magnetic alginate beads for Pb (II) ions removal from wastewater, J. Colloid Interface Sci. 362 (2011) 486–492, https://doi.org/10.1016/j.jcis.2011.06.036.

[27] V. Rocher, A. Bee, J.M. Siaugue, V. Cabuil, Dye removal from aqueous solution by magnetic alginate beads crosslinked with epichlorohydrin, J. Hazard. Mater. 178 (2010) 434–439, https://doi.org/10.1016/j.jhazmat.2010.01.100.

[28] P. Majumdar, A.Y. Khan, R. Bandyopadhyaya, Diffusion, adsorption and reaction of glucose in glucose oxidase enzyme immobilized mesoporous silica (SBA-15) particles: experiments and modelling, Biochem. Eng. J. 105 (2016) 489–496, https://doi.org/10.1016/j.bej.2015.10.011.

[29] G. Germanos, S. Youssef, M. Abboud, W. Farah, B. Lescopc, S. Rioual, Diffusion and agglomeration of iron oxide nanoparticles in magnetic calcium alginate beads initiated by copper sorption, J. Environ. Chem. Eng. 5 (2017) 3727–3733, https://doi.org/10.1016/j.jece.2017.07.033.

[30] Z.W. Ouyang, E.C. Chen, T.M. Wu, Thermal stability and magnetic properties of polyvinylidene Fluoride/Magnetite nanocomposites, Materials 8 (2015) 4553–4564, https://doi.org/10.3390/ma8074553.

[31] S. Mandal, S.S. Kumar, B. Krishnamoorthy, S.K. Basu, Development and evaluation of calcium alginate beads prepared by sequential and simultaneous methods, Braz. J. Pharm. Sci. 46 (2010) 785–793, https://doi.org/10.1590/S1984-82502010000400021.

[32] M.M. Shahri, S. Azizi, Design, Optimization Process and Efficient Analysis for Preparation of Copolymer-Coated Superparamagnetic Nanoparticles, J. Nanostructure Chem. 7 (3) (2017) 205–215.
[33] S.J. Kemp, R.M. Ferguson, A.P. Khandhar, K.M. Krishnan, Monodisperse magnetite nanoparticles with nearly ideal saturation magnetization, RSC Adv. 6 (2016) 77452–77464, https://doi.org/10.1039/C6RA12072E.
[34] A.A. Bakr, Y.M. Moustafa, E.A. Motawea, M.M.H. Khalil, M.M. Yehia, Magnetic nanocomposite beads: synthesis and uptake of Cu(II) ions from aqueous solutions, Can. J. Chem. 93 (3) (2015) 289–296, https://doi.org/10.1139/cjc-2014-0282.
[35] Y.S. Ho, G. McKay, Kinetic model for lead (II) sorption onto peat, Adsorp. Sci. Technol. 16 (1998) 243–255, https://doi.org/10.1177/026361749801600401.
[36] C.T. Miller, W.J. Weber Jr., Sorption of hydrophobic organic pollutants in saturated soil systems, J. Contam. Hydrol. 1 (1986) 243–261, https://doi.org/10.1016/0169-7722(86)90019-7.
[37] F. Fu, Q. Wang, Removal of heavy metal ions from wastewaters: a review, J. Environ. Manage. 92 (2011) 407–418, https://doi.org/10.1016/j.jenvman.2010.11.011.
[38] H. Zhu, Y. Fu, R. Jiang, J. Yao, L. Xiao, G. Zeng, Optimization of copper(II) adsorption onto novel magnetic calcium Alginate/Maghemite hydrogel beads using response surface methodology, Ind. Eng. Chem. Res. 53 (10) (2014) 4059–4066, https://doi.org/10.1021/ie4031677.
[39] A. Ely, M. Baudu, M.O.S. Ould Kankou, J.P. Basly, Copper and nitrophenol removal by low cost alginate/Mauritanian clay composite beads, Chem. Eng. J. 178 (15) (2011) 168–174, https://doi.org/10.1016/j.cej.2011.10.040.
[40] J. Wang, L. Xu, Y. Meng, C. Cheng, A. Li, Adsorption of Cu^{2+} on new hypercrosslinked polystyrene adsorbent: batch and column studies, Chem. Eng. J. 178 (2011) 108–114, https://doi.org/10.1016/j.cej.2011.10.022.
[41] S.A. Tawfik, N.S. Mohammad, A.A. Abdurrahman, Kinetic and intraparticle diffusion studies of carbon nanotubes-titania for desulfurization of fuels, Pet. Sci. Technol. 34 (16) (2016) 1468–1474, https://doi.org/10.1080/10916466.2016.1202972.
[42] E.G. Deze, S.K. Papageorgiou, E.P. Favvas, F.K. Katsaros, Porous alginate aerogel beads for effective and rapid heavy metal sorption from aqueous solutions: effect of porosity in Cu^{2+} and Cd^{2+} ion sorption, Chem. Eng. J. 209 (2012) 537–546, https://doi.org/10.1016/j.cej.2012.07.133.
[43] S. Peretz, D.F. Anghel, E. Vasilescu, Synthesis, characterization and adsorption properties of alginate porous beads, Polym. Bull. Berl. (Berl) 72 (2015) 3169–3182, https://doi.org/10.1007/s00289-015-1459-4.
[44] S. Wierzba, Biosorption of nickel (II) and zinc (II) from aqueous solutions by the biomass of yeast Yarrowia lipolytica, Polish J. Chem. Technol. 19 (1) (2017) 1–10, https://doi.org/10.1515/pjct-2017-0001.
[45] S. Vahidhabanu, D. Karuppasamy, A.I. Adeogun, B.R. Babu, Impregnation of zinc oxide modified clay over alginate beads: a novel material for the effective removal of congo red from wastewater, RSC Adv. 7 (2017) 5669–5678, https://doi.org/10.1039/C6RA26273B.